Applied Catalysis B: Environmental 176–177 (2015) 325–330

Contents lists available at ScienceDirect

Applied Catalysis B: Environmental

journal homepage: www.elsevier.com/locate/apcatb

Highly efficient reduction of hexavalent chromium on amino-functionalized palladium nanowires

Ling-Ling Wei [a], Rui Gu [a], Jong-Min Lee [b,*]

[a] School of Chemistry and Chemical Engineering, Shaanxi Normal University, Xi'an 710062, PR China
[b] School of Chemical and Biomedical Engineering, Nanyang Technological University, Singapore, 637459, Singapore

ARTICLE INFO

Article history:
Received 23 January 2015
Received in revised form 18 March 2015
Accepted 30 March 2015
Available online 9 April 2015

Keywords:
Palladium nanowires
Chemical functionalization
Oriented attachment
Hexavalent chromium reduction
Formic acid

ABSTRACT

Palladium (Pd) nanostructures are attracting much attention due to their intriguing optical, electrical, and catalytic properties. Pd-catalytic hydrogenation is an effective route for remediating organic and inorganic contaminants. In this work, a simple formate-mediated chemical reduction method is used to synthesize the polyallylamine functionalized Pd nanowire networks (Pd-NWWs). The morphology, structure, and surface composition of Pd-NWWs are investigated in detail. The formation mechanism of Pd-NWWs is defined in accordance with the experimental observation and discussion. Physical characterization shows the as-synthesized products are a three-dimensionally interconnected network with one-dimensional Pd nanowires as building blocks, and the Pd nanowires grow from the primary spherical Pd nanocrystals via the oriented attachment. In comparison with commercial Pd black, the amino-functionalized Pd-NWWs exhibit remarkably improved catalytic activity for the hexavalent chromium reduction at room temperature.

1. Introduction

Hexavalent chromium (Cr^{VI}) compounds have wide industrial applications in metal finishing, wood products, electroplating, and dye production, etc [1–4]. However, Cr^{VI} compounds which increase the risk of DNA mutation and lung cancer via chronic inhalation are highly toxic, mutagenic, and carcinogenic. Conversely, trivalent chromium (Cr^{III}) is nontoxic and relatively inert, and trace amount of Cr^{III} is an essential nutrient for humans and other animals. For remediating Cr^{VI} contamination, the reductive transformation of Cr^{VI} to Cr^{III} is a promising alternative approach to the existing noncatalytic treatment methods, such as adsorption, electrochemical treatment, membrane filtration, and ion exchange [5–9].

Palladium (Pd) nanostructures, a widely applied metal nanomaterial in catalysis, are highly active for the catalytic-hydrogenolysis of organohalogen compounds and catalytic-reduction of heavy metal pollutants [4,10]. Recently, Pd-catalytic reduction of Cr^{VI} by formic acid has attracted great interest due to its simplicity and efficiency [10–19]. In principle, formic acid undergoes a dehydrogenation decomposition pathway to produce H_2 and CO_2 ($HCOOH \rightarrow CO_2 + H_2$) [19–23]. Then, H_2 adsorbed on a Pd surface consequently reduces Cr^{VI} to Cr^{III} via a H_2 transfer pathway ($Cr_2O_7^{2-} + 8H^+ + 3H_2 \rightarrow 2Cr^{3+} + 7H_2O$) [12,18].

As it is well known, the intrinsic catalytic activity of Pd nanostructures can be highly improved by controlling their morphology and surface composition due to the crystal face effect and synergistic effect between different components [24–30]. In this work, we develop a facile and efficient route to synthesize polyallylamine (PAH) functionalized Pd nanowire networks (Pd-NWWs) with a high yield in an aqueous solution. The formation of Pd-NWWs is remarkably promoted by introducing high concentrated sodium formate into the reaction system. When used as a catalyst for the reduction of Cr^{VI}, the as-synthesized amino-functionalized Pd-NWWs show remarkably improved catalytic performance compared with commercial Pd black at room temperature.

2. Experimental

2.1. Reagents and chemicals

PAH (Scheme 1, MW: 15 0000) was purchased from Nitto Boseki Co., Ltd. Potassium tetrachloropalladate(II) (K_2PdCl_4), sodium formate (HCOONa), hydrazine hydrate ($N_2H_4{\cdot}H_2O$), formic acid (HCOOH), and potassium dichromate ($K_2Cr_2O_7$) were supplied

* Corresponding author. Tel.: +65 65138129.
E-mail address: jmlee@ntu.edu.sg (J.-M. Lee).

http://dx.doi.org/10.1016/j.apcatb.2015.03.056
0926-3373/

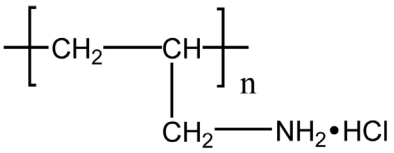

Scheme 1. Molecular structure of PAH.

from Sinopharm Chemical Reagent Co., Ltd. Commercial Pd black was purchased from Johnson Matthey Corporation.

2.2. Preparation of Pd nanowire networks (Pd-NWWs)

9.0 mL of 0.05 M PAH (molarity of PAH given with respect to the repeating unit) and 1.0 mL of 0.05 M K_2PdCl_4 aqueous solutions were added into 8.0 mL of water with continued stirring (pH 7.0). Then, 8.0 g of HCOONa was added into the mixture solution and stirred for 1.5 h at 80 °C. After the reaction, the obtained Pd-NWWs were separated by centrifugation, washed and then dried. Finally, the Pd-NWWs were further treated with UV/ozone for 4 h (note: PAH could not be easily removed because of the excellent chemical stability of PAH, which was confirmed by XPS and FT-IR in the previous works) [29,31].

2.3. Instruments

The morphology and bulk composition of the Pd-NWWs were characterized by JSM-2010 scanning electron microscopy (SEM), JEM-2100F transmission electron microscopy (TEM), and energy dispersive X-ray (EDX) spectrum. Crystal structure and surface composition of the Pd-NWWs were investigated by Model D/max-rC X-ray diffraction (XRD) diffractometer, Nicolet 520 SXFTIR Fourier transform infrared (FT-IR) spectrophotometer, and Thermo VG Scientific ESCALAB 250 X-ray photoelectron spectroscopy (XPS). The binding energy was calibrated by means of the C 1s peak energy of 284.6 eV. The reduction process of Cr^{VI} was monitored using a Shimadzu 3600 ultraviolet and visible spectroscopy (UV–vis) spectrophotometer.

2.4. Electrochemical measurements

Electrochemical tests were performed on a CHI 660C electrochemical workstation. A three-electrode system (which was assembled with a platinum wire as the auxiliary electrode, a saturated calomel electrode (SCE) as the reference electrode, and a catalyst modified glassy carbon (GC) electrode as the working electrode) was used for all electrochemical tests. The Nafion covered catalyst modified electrode was prepared according to the procedure reported previously [32]. The loading of Pd metal on the work electrode was 51 $\mu g\,cm^{-2}$. Cyclic voltammetry measurements were conducted in a N_2-saturated 0.1 M $HClO_4$ solution. In order to avoid the interference of the hydrogen absorption in bulk Pd, the surface areas of the Pd catalysts were measured by integrating a reduction charge of surface palladium oxide and assuming a value of 420 $\mu C\,cm^{-2}$ for the reduction charge of a palladium oxide monolayer [33].

2.5. Catalytic reduction of Cr^{VI}

For the reduction of Cr^{VI}, $K_2Cr_2O_7$ was the source of Cr^{VI} and HCOOH was the electron donor under an acidic solution. Typically, 20 μL of Pd-NWWs aqueous solution (2.0 $g\,L^{-1}$) was added into 10 mL of 0.8 mM $K_2Cr_2O_7$ + 0.45 M HCOOH mixture solution under gentle magnetic stirring. The reaction process was monitored by measuring the UV–Vis' absorbance of $K_2Cr_2O_7$ at 350 nm. For comparison, commercial Pd black was used as the catalyst for the catalytic reduction of Cr^{VI}.

3. Results and discussion

3.1. Characterization of Pd-NWWs

The amino-functionalized Pd-NWWs were readily achieved by reducing K_2PdCl_4 with HCOONa in the presence of PAH at 80 °C for 1.5 h (see Section 2 for details). The SEM image shows the existence of pores and the network-like morphology is observed (Fig. 1A). EDX measurement shows that the products contain mainly the Pd

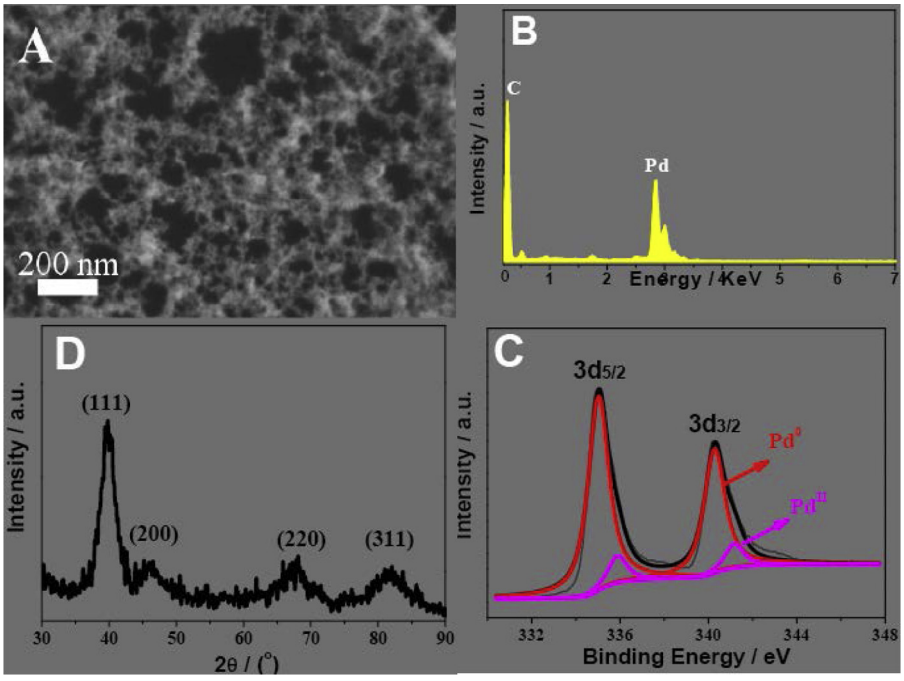

Fig. 1. (A) SEM image, (B) EDX spectrum, (C) Pd 3d XPS spectrum, and (D) XRD pattern of Pd-NWWs.

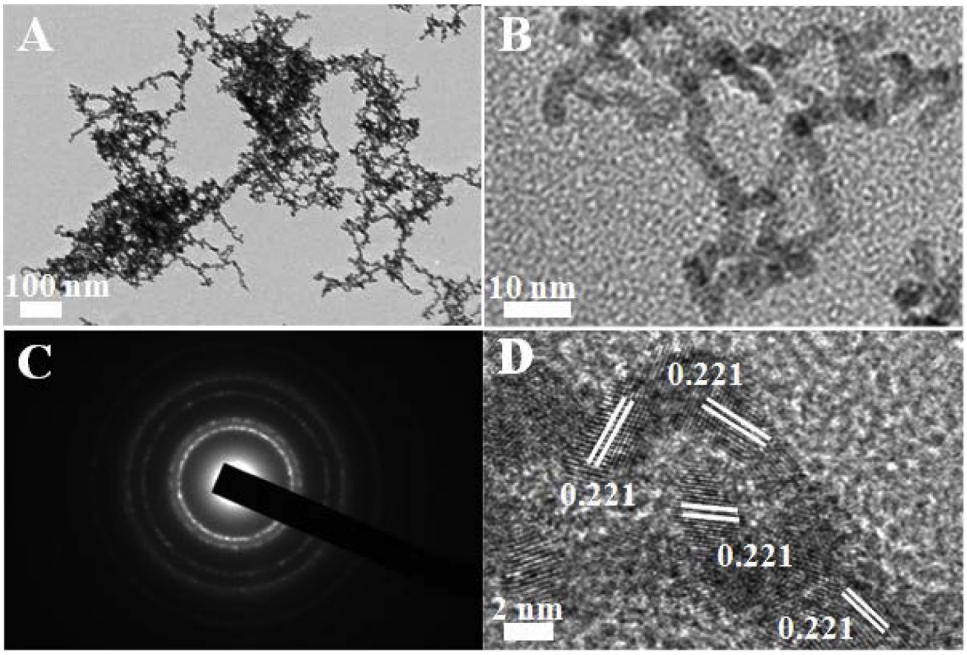

Fig. 2. (A) Typical TEM image, (B) magnified TEM image, (C) SAED pattern and (D) HR-TEM image of Pd-NWWs.

element (Fig. 1B). Further XPS spectrum indicates the percentage of Pd^0 species in the products is 89 % (Fig. 1C), demonstrating that the Pd^{II} precursor is reduced by HCOONa. The XRD pattern shows that the as-prepared Pd networks have four peaks corresponding to the (1 1 1), (2 0 0), (2 2 0), and (3 1 1) facets of face-centered cubic (fcc) Pd crystal (JCPDS standard 5-681 Pd), indicating their fcc structure (Fig. 1D). The ratio between the intensity of the (1 1 1) and (2 0 0) peaks is higher than the standard value of JCPDS 5-681Pd (3.90 versus 2.38), indicating that Pd-NWWs have abundant Pd (1 1 1) facets [29].

The morphology and structure of the as-synthesized Pd-NWWs were further characterized by TEM. The TEM images show that the Pd-NWWs consist of Pd nanowires with an average diameter of 3.5 ± 1.0 nm and length of a few tens of nanometers (Fig. 2A and B). The selected area electron diffraction (SAED) pattern of the Pd-NWWs shows the discrete diffraction rings (Fig. 2C), suggesting that the Pd-NWWs are polycrystalline. Further the high resolution TEM (HR-TEM) image shows the d-spacing of 0.221 nm (Fig. 2D), which is close to the (1 1 1) inter-planar distance of fcc Pd (0.226 nm). Mainly, PAH preferentially binds onto the (1 1 1) facets of Pd nanocrystals, resulting in the restricted growth of the (11 1) facets [29]. Moreover, it is clearly observed that fringes are discontinuous, predicting the oriented attachment grown mechanism [34].

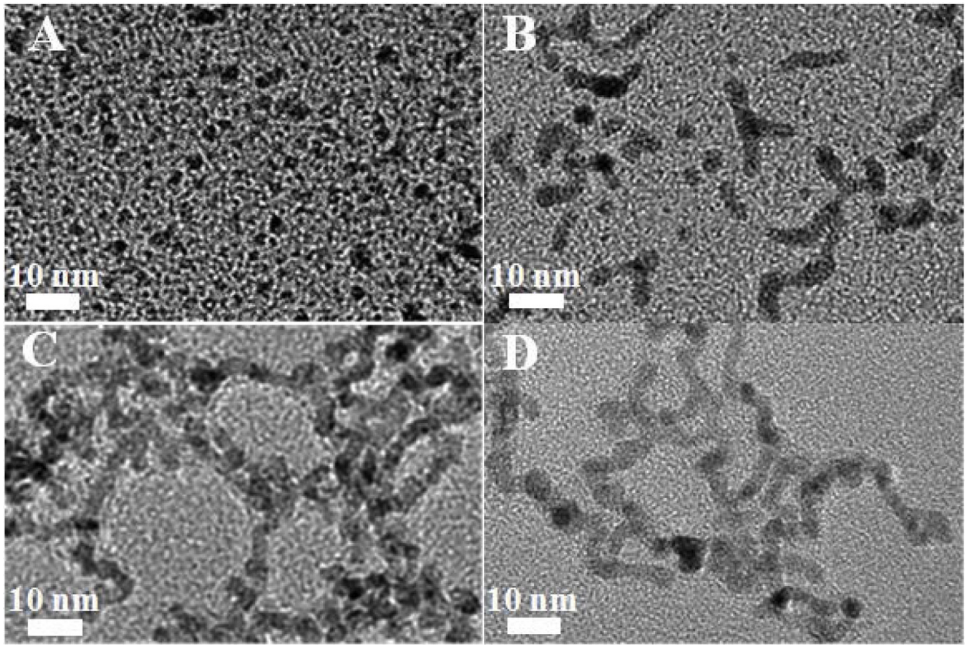

Fig. 3. TEM images of Pd-NWWs synthesized at a reaction time of (A) 30, (B) 50, (C) 70, and (D) 90 min.

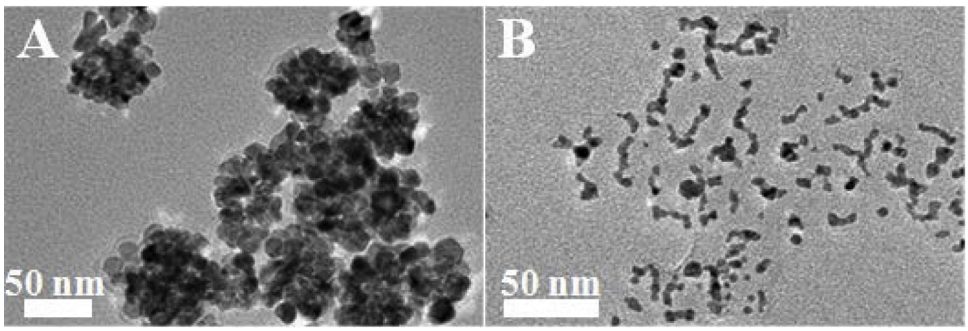

Fig. 4. (A) TEM image of Pd nanodendrites obtained by using $N_2H_4{\cdot}H_2O$ as reducing agent. (B) TEM image of short Pd nanorods obtained by using the low concentration of HCOONa as a reducing agent.

3.2. Formation mechanism of Pd-NWWs

In order to explore the growth mechanism of Pd-NWWs, the reaction intermediates were collected and characterized by TEM. At the initial 30 min, a lot of irregular Pd nanocrystals (less than 4 nm in diameter) are found (Fig. 3A). When the reaction time increases to 50 min, a number of small Pd nanocrystals disappear and Pd nanorods begin to appear together with the elongated nanocrystals (Fig. 3B). Further increasing reaction time to 70 min, the long Pd nanonecklaces which consist of the spherical Pd nanocrystals are clearly observed (Fig. 3C). At the end of 90 min, well-defined Pd nanowires are fully formed, and no single Pd nanocrystal is found (Fig. 3D). During the evolution process, the diameter of Pd nanowires changes very little. Thus, the morphological change from sphere to wire with the increase in reaction time strongly confirms that the oriented attachment mechanism is responsible for the generation of Pd nanowires [34,35].

To further explore the driving force for oriented attachment, a series of controlled experiments were conducted. When $N_2H_4{\cdot}H_2O$ is used as the reducing agent, Pd nanodendrites are obtained (Fig. 4A). In pH 7.0 solution, N_2H_4 exists as a positively charged $N_2H_5^+$ cation, whereas, HCOONa exists as a negatively charged $HCOO^-$ anion. Thus, we infer that the reducing agent with negative charge plays an important role for the formation of Pd nanowires. With the low concentration of HCOONa, a lot of Pd nanocrystals are obtained, and some of them assemble into a short rod-like shaped structure, but no long Pd nanowires are obtained (Fig. 4B). This fact further indicates a high concentrated $HCOO^-$ anion can effectively serve as a linker agent to drive Pd nanocrystals to self-connect.

A recent work indicated PAH strongly bound Pd (1 1 1) facets and resulted in the growth of Pd (1 1 1) facets [29]. In the present synthesis, the amino-functionalization of Pd-NWWs was confirmed by XPS. The appearance of N 1s at 399.5 eV implies the adsorption of PAH on Pd-NWWs' surface (Fig. 5A). The FT-IR spectrum of pure PAH is close to that of as-prepared Pd-NWWs (Fig. 5B), further confirming that the Pd-NWWs are covered with PAH molecules due to the strong N—Pd bond interaction [29]. The amino-functionalization of the Pd-NWWs was further visualized by EDX mapping. The Pd element pattern is similar to the N element pattern (Fig. 5C), suggesting the uniform binding of PAH on the Pd-NWWs' surface. At pH 3.0, the zeta potential of Pd-NWWs is measured to be +36 mV, indicating the overall surface of Pd-NWWs has distributed positively charged $-NH_3^+$ groups.

During the growth of Pd-NWWs, these positive charges on the Pd crystal nuclei surface prevent the preformed Pd crystal nuclei from coming together to aggregate. However, thermal

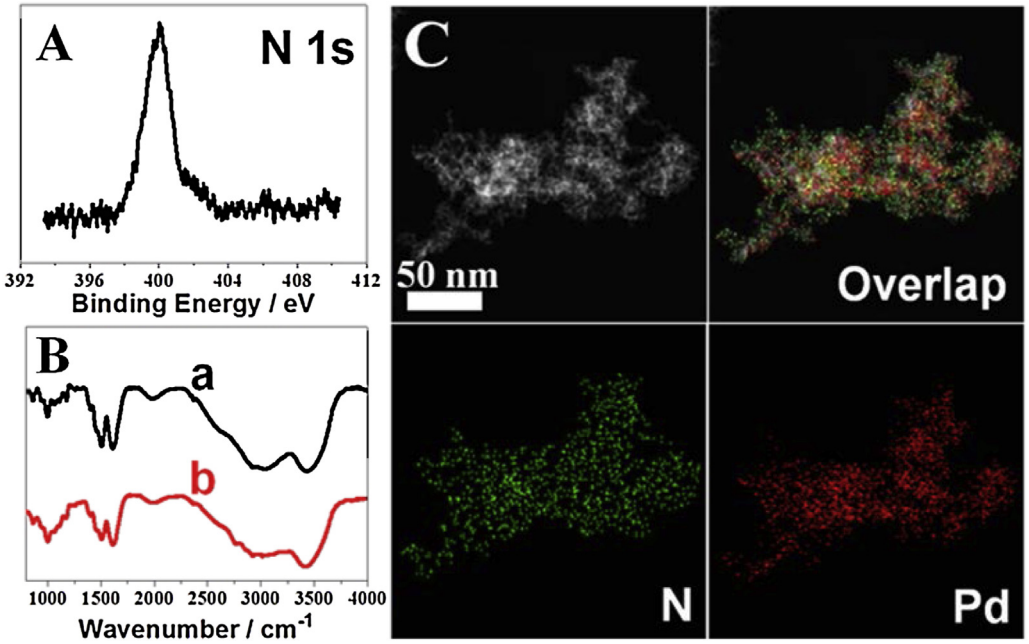

Fig. 5. (A) XPS spectrum of Pd-NWWs in the N1s region. (B) FT-IR spectra of (a) Pd-NWWs and (b) bulk PAH. (C) EDX mapping patterns of Pd-NWWs. (C) EDX mapping images of Pd-NWWs.

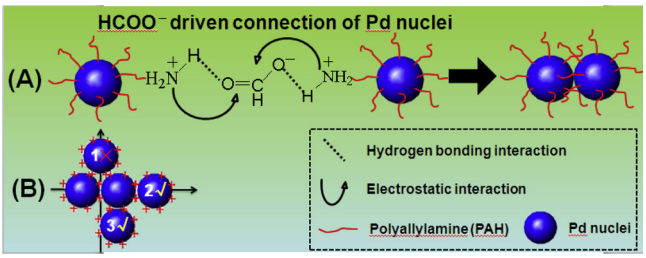

Scheme 2. (A) Electrostatic and/or hydrogenbonding induced connection of Pd crystal nuclei. (B) Growth mechanism of the spherical Pd nanoparticles to form the wire-like morphology.

perturbation can overcome the repulsion barrier and achieve an aggregation of two spherical nanocrystals when the charge repulsion between the two nanocrystals decreases under certain conditions. Owing to electrostatic and/or hydrogen bonding interactions between $HCOO^-$ and $-NH_3^+$ groups on PAH, the first two PAH functionalized Pd crystal nuclei may associate with each other, forming the "primary unit" of the nanowires (Scheme 2A). According to the electrostatic repulsion, the third PAH functionalized Pd crystal nucleus prefers to aggregate at position 2 or 3 rather than position 1, to generate nanowires (Scheme 2B) [36]. Specifically, the position 1 has the highest electrostatic repulsion for the third Pd crystal nucleus because this position has the most positive charge in contact with the neighboring crystal nuclei. Therefore, the third PAH functionalized Pd crystal nucleus preferentially selects position 2 or 3 with less electrostatic repulsion to self-connect via electrostatic and/or hydrogenbonding interactions between $HCOO^-$ and $-NH_3^+$ on PAH, and consequently results in the formation of Pd nanowires.

3.3. Catalytic performance of Pd-NWWs

The catalytic activities of Pd-NWWs and Pd black for the Cr^{VI} reduction by HCOOH were investigated by monitoring the characteristic absorption peak of Cr^{VI} at 350 nm using a UV–vis spectrophotometer [18,23]. In the absence of a catalyst, the Cr^{VI} aqueous solution containing HCOOH does not show the obvious decrease in the absorption intensity at 350 nm within 480 min (Fig. 6A), indicating the reduction of Cr^{VI} cannot proceed without the Pd catalyst. In the presence of Pd-NWWs and Pd black, the characteristic absorption peak of Cr^{VI} gradually decreases and vanishes within 15 min (Fig. 6B) and 230 min (Fig. 6C), suggesting the successful conversion of Cr^{VI} to Cr^{III}. Reaction rate constant κ for Pd-NWWs and Pd black was calculated from the slope of the plots of $\ln(C_t/C_0)$ versus reaction time (t), respectively (Fig. 6D). The reduction rate of Cr^{VI} to Cr^{III} on Pd-NWWs (κ: 0.282 min^{-1}) is 16.9 times faster than that on Pd black (κ: 0.0167 min^{-1}) at room temperature. To further evaluate the catalytic performance of catalyts, the turnover frequencies (TOF, defined as the number of Cr^{VI} per metallic Pd per minute based on the total mass of metallic Pd, the unit is $mol^1\ mol^{-1}\ min^{-1}$) of the Pd-NWWs and Pd black were calculated to be 151.1 and 10.0 $mol^1\ mol^{-1}\ min^{-1}$, respectively. Compared with the recently reported PVP-Pd_{10} catalyst (TOF: 22.2 $mol^1\ mol^{-1}\ min^{-1}$) and Pd-$Fe_3O_4$ catalyst (TOF: 7.45 $mol^1\ mol^{-1}\ min^{-1}$) [37], the Pd-NWWs show more competitive catalytic activity.

It is well known that the catalytic performance of catalyst highly relates with its surface area. The previous work indicated the PAH molecules on the surface of Pd nanoparticles severely affected the nitrogen adsorption–desorption [38]. Thus, electrochemical method was used to determine the surface areas of the Pd-NWWs and Pd black. Surprisingly, the electrochemical measurements show the surface area (17.1 $m^2\ g^{-1}$) of the Pd-NWWs is only 1.99 times larger than that (8.6 $m^2\ g^{-1}$) of the Pd black (Fig. 7). Thus, the improved catalytic activity of the Pd-NWWs for the Cr^{VI} reduction cannot be simply attributed to the area effect. As confirmed by XPS, FT-IR, and EDX mapping spectra, PAH exists at Pd-NWWs' surface. Under acidic conditions, the $-NH_2$ groups on PAH can be easily protonated and form positively charged $-NH_3^+$ groups. By

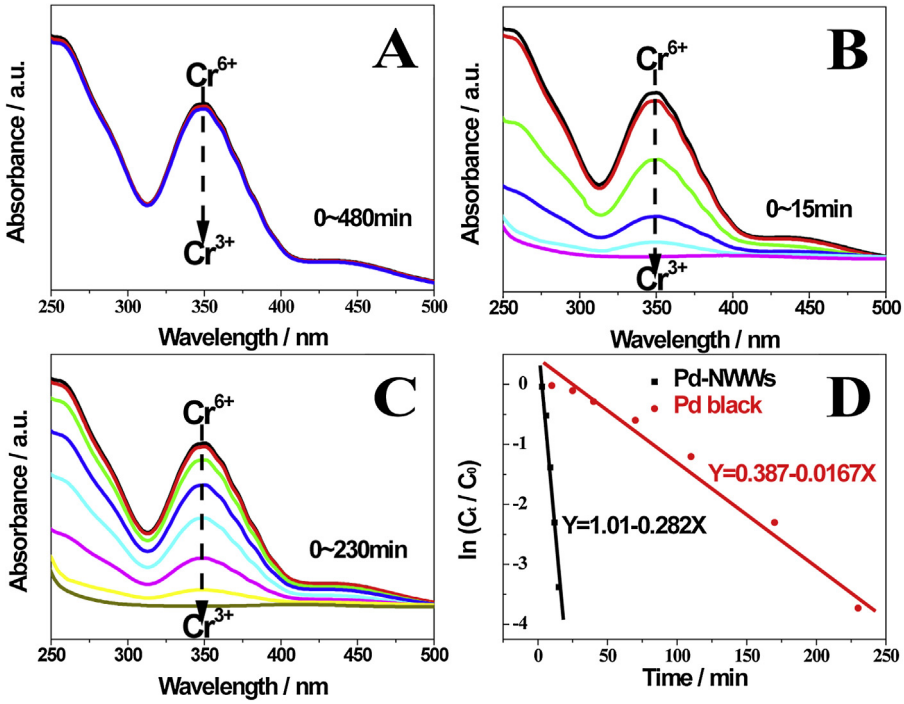

Fig. 6. UV–vis spectra for successive reduction of $Cr_2O_7^{2-}$ with HCOOH at room temperature: (A) catalyst-free, (B) catalyzed by Pd-NWWs, (C) catalyzed by commercial Pd black, (D) the relationship between $\ln(C_t/C_0)$ and reaction time (t).

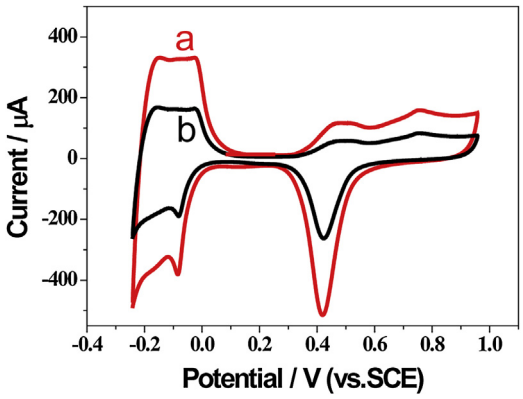

Fig. 7. Cyclic voltammograms of (a) Pd-NWWs/GC and (b) Pd-black/GC electrodes in N_2-saturated 0.1 M $HClO_4$ solution at a scan rate of 50 mV s^{-1}.

the electrostatic interaction, the $-NH_3^+$ groups on the Pd-NWWs sufficiently attract the negatively charged $Cr_2O_7^{2-}$ and $HCOO^-$ ions, resulting in the enrichment of $Cr_2O_7^{2-}$ and $HCOO^-$ ions on the surface of the Pd-NWWs [39], which may be responsible for improved catalytic activity of the Pd-NWWs. Meanwhile, the Pd-NWWs have the particular advantages: for example, the 1D nanowire building blocks accelerate electron transport in the course of the redox reaction [40,41], and 3D configuration of the Pd-NWWs facilitates the mass transport of reagents [32,42]. Additionally, recent theoretical calculations on the HCOOH decomposition on Pd (1 1 1) unanimously demonstrated that the dehydrogenation involved a much lower barrier than the dehydration pathway [20–22]. Thus, H_2 is proposed as the highly preferred product for the HCOOH decomposition on the (1 1 1)–facet enclosed Pd-NWWs, and consequently reduces Cr^{VI} to Cr^{III} through H_2 transfer, which also contributes to the improved catalytic activity of the Pd-NWWs. Furthermore, the stability of the Pd-NWWs was also evaluated. After six catalysis cycles, no obvious loss of activity is observed, indicating the excellent durability. Likely, the particular 3D interconnected structure of the Pd-NWWs effectively restrains their Ostwald ripening effect, and consequently contributes to the good stability [32,42].

4. Conclusions

In summary, we presented a facile and mild chemical reduction route (e.g., 1.5 h, 80 °C, and aqueous solution) to synthesize the amino-functionalized Pd-NWWs via an oriented attachment grown mechanism. During the process, HCOONa not only acted as a reducing agent to reduce K_2PdCl_4 but also assisted the self-connection of PAH functionalized Pd nanocrystals via electrostatic and/or hydrogen bonding interactions between $HCOO^-$ and $-NH_3^+$ groups on PAH, resulting in the formation of Pd nanowires. Additionally, the amino-functionalized Pd-NWWs exhibited remarkably improved catalytic performance for Cr^{VI} reduction compared with the commercial Pd black owing to the particular 3D interconnected structure of the Pd-NWWs and the synergistic catalytic effect between the PAH and Pd-NWWs.

Acknowledgments

This work was supported by China Postdoctoral Science Foundation (2014M562367), the Fundamental Research Fund for the Central Universities (GK261001304), and the Academic Research Fund of the Ministry of Education in Singapore (RGT27/13).

References

[1] K. Bhowmik, A. Mukherjee, M.K. Mishra, G. De, Langmuir 30 (2014) 3209–3216.
[2] K.K. Krishnani, S. Srinives, B. Mohapatra, V.M. Boddu, J. Hao, X. Meng, A. Mulchandani, J. Hazard. Mater. 252 (2013) 99–106.
[3] Y. Tian, L. Huang, X. Zhou, C. Wu, J. Hazard. Mater. 225–226 (2012) 15–20.
[4] A. Qian, P. Liao, S. Yuan, M. Luo, Water Res. 48 (2014) 326–334.
[5] O.A. Sadik, N.M. Noah, V.A. Okello, Z. Sun, J. Chem. Educ. 91 (2014) 269–273.
[6] Y. Guo, D. Wang, X. Liu, X. Wang, W. Liu, W. Qin, New J. Chem. 38 (2014) 5861–5867.
[7] B.J. Borah, H. Saikia, P. Bharali, New J. Chem. 38 (2014) 2748–2751.
[8] M.A. Omole, V.A. Okello, V. Lee, L. Zhou, O.A. Sadik, C. Umbach, B. Sammakia, ACS Catal. 1 (2011) 139–146.
[9] M. Rivero-Huguet, W.D. Marshall, J. Hazard. Mater. 169 (2009) 1081–1087.
[10] C. Yang, J.H. Meldon, B. Lee, H. Yi, Catal. Today 233 (2014) 108–116.
[11] M. Liang, R. Su, W. Qi, Y. Zhang, R. Huang, Y. Yu, L. Wang, Z. He, Ind. Eng. Chem. Res. 53 (2014) 13635–13643.
[12] G.T. Fu, X. Jiang, R. Wu, S.H. Wei, D.M. Sun, Y.W. Tang, T.H. Lu, Y. Chen, ACS Appl. Mater. Interfaces 6 (2014) 22790–22795.
[13] M. Yadav, Q. Xu, Chem. Commun. 49 (2013) 3327–3329.
[14] H. Chen, Y. Shao, Z. Xu, H. Wan, Y. Wan, S. Zheng, D. Zhu, Appl. Catal. B-Environ. 105 (2011) 255–262.
[15] I.O. K'Owino, M.A. Omole, O.A. Sadik, J. Environ. Monit. 9 (2007) 657–665.
[16] C. Yang, A.K. Manocchi, B. Lee, H. Yi, Appl. Catal. B-Environ. 93 (2010) 282–291.
[17] C. Yang, C.-H. Choi, C.-S. Lee, H. Yi, ACS Nano 7 (2013) 5032–5044.
[18] Y. Huang, H. Ma, S. Wang, M. Shen, R. Guo, X. Cao, M. Zhu, X. Shi, ACS Appl. Mater. Interfaces 4 (2012) 3054–3061.
[19] M.A. Omole, I.O. K'Owino, O.A. Sadik, Appl. Catal. B-Environ. 76 (2007) 158–167.
[20] R. Zhang, H. Liu, B. Wang, L. Ling, J. Phys. Chem. C 116 (2012) 22266–22280.
[21] K. Mori, M. Dojo, H. Yamashita, ACS Catal. 3 (2013) 1114–1119.
[22] C. Hu, S.-W. Ting, K.-Y. Chan, W. Huang, Int. J. Hydrogen Energy 37 (2012) 15956–15965.
[23] A. Dandapat, D. Jana, G. De, Appl. Catal. A-Gen. 396 (2011) 34–39.
[24] A. Bulut, M. Yurderi, Y. Karatas, M. Zahmakiran, H. Kivrak, M. Gulcan, M. Kaya, Appl. Catal. B-Environ. 164 (2015) 324–333.
[25] Y. Diao, P. Yang, R. Yan, L. Jiang, L. Wang, H. Zhang, C. Li, Z. Li, S. Zhang, Appl. Catal. B-Environ. 142–143 (2013) 329–336.
[26] Z. Dong, X. Le, C. Dong, W. Zhang, X. Li, J. Ma, Appl. Catal. B-Environ. 162 (2015) 372–380.
[27] K. Jiang, W.-B. Cai, Appl. Catal. B-Environ. 147 (2014) 185–192.
[28] Z. Zhao, Y.-L. Fang, P.J.J. Alvarez, M.S. Wong, Appl. Catal. B-Environ. 140–141 (2013) 468–477.
[29] G. Fu, X. Jiang, L. Tao, Y. Chen, J. Lin, Y. Zhou, Y. Tang, T. Lu, Langmuir 29 (2013) 4413–4420.
[30] G. Fu, X. Jiang, L. Ding, L. Tao, Y. Chen, Y. Tang, Y. Zhou, S. Wei, J. Lin, T. Lu, Appl. Catal. B-Environ. 138–139 (2013) 167–174.
[31] G. Fu, X. Jiang, M. Gong, Y. Chen, Y. Tang, J. Lin, T. Lu, Nanoscale 6 (2014) 8226–8234.
[32] L. Zhang, D. Lu, Y. Chen, Y. Tang, T. Lu, J. Mater. Chem. A 2 (2014) 1252–1256.
[33] M. Zheng, P. Li, G. Fu, Y. Chen, Y. Zhou, Y. Tang, T. Lu, Appl. Catal. B-Environ. 129 (2013) 394–402.
[34] J. Xu, G. Fu, Y. Tang, Y. Zhou, Y. Chen, T. Lu, J. Mater. Chem. 22 (2012) 13585–13590.
[35] M. Xiao, S. Li, J. Zhu, K. Li, C. Liu, W. Xing, ChemPlusChem 79 (2014) 1123–1128.
[36] S. Yang, X. Yu, L. Wang, Y. Tu, J.X. Zheng, J. Xu, R.M. Van Horn, S.Z.D. Cheng, Macromolecules 43 (2010) 3018–3026.
[37] W. Tu, K. Li, X. Shu, W.Y. William, J. Nanopart. Res. 15 (2013) 1–9.
[38] G. Fu, W. Han, L. Yang, J. Lin, S. Wei, Y. Chen, Y. Zhou, Y. Tang, T. Lu, X. Xia, J. Mater. Chem. 22 (2012) 17604–17611.
[39] L. Wang, W. Liu, T. Wang, J. Ni, Chem. Eng. J. 225 (2013) 153–163.
[40] M. Chen, B. Wu, J. Yang, N. Zheng, Adv. Mater. 24 (2012) 862–879.
[41] W. Hong, J. Wang, E. Wang, Int. J. Hydrogen Energy 39 (2014) 3226–3230.
[42] X. Liu, G. Fu, Y. Chen, Y. Tang, P. She, T. Lu, Chem. Eur. J. 20 (2014) 585–590.